Editors' Suggestion

Experimental Demonstration of Mode-Coupled and High-Brightness Self-Amplified Spontaneous Emission in an X-Ray Free-Electron Laser

Eduard Prat,[1,*] Wenxiang Hu,[1,2] Christopher Arrell,[1] Marco Calvi,[1] Philipp Dijkstal,[1] Rolf Follath,[1] and Sven Reiche[1]

[1]Paul Scherrer Institut, CH-5232 Villigen, Switzerland

[2]Laboratory for Solid State Physics and Quantum Center, ETH Zürich, CH-8093 Zürich, Switzerland

(Received 19 July 2024; accepted 4 October 2024; published 12 November 2024)

X-ray free-electron lasers (FELs) are modern research tools with applications in multiple scientific fields. Standard x-ray FEL pulses are produced by the self-amplified spontaneous emission (SASE) mechanism. SASE-FEL pulses have high power, short duration, and excellent transverse coherence but exhibit poor temporal coherence with power and spectral profiles consisting of multiple randomly distributed spikes. Here, we present the demonstration of two modes that enhance the temporal coherence of SASE-FEL radiation: mode-coupled and high-brightness SASE. Both schemes are based on delaying the electron beam with magnetic chicanes placed between the undulator modules of the FEL facility. First, we show the generation of frequency combs with tunable peak separation via the mode-coupled SASE scheme. Second, we present a proof-of-principle demonstration of the high-brightness SASE mechanism, producing FEL pulses with a bandwidth reduction up to a factor of 3 with respect to standard SASE pulses. The demonstration was done at Athos, the soft x-ray beamline of SwissFEL, for photon energies between 500 and 600 eV. Our work will benefit current applications and may open up new research areas requiring frequency combs or narrow bandwidths.

DOI: 10.1103/PhysRevLett.133.205001

X-ray free-electron lasers (FELs) are cutting-edge research instruments capable of studying matter with time and spatial resolution at the scale of atomic processes [1–10]. In an x-ray FEL, a high-brightness electron beam with multi-GeV energy travels through an undulator to produce the FEL radiation. X-ray FELs generate radiation pulses with peak powers of tens of GW or higher, and durations of several tens of femtoseconds or shorter. Most of the x-ray FEL facilities are based on the self-amplified spontaneous emission (SASE) process [11,12], which starts from the shot noise of the electron beam. The SASE process results in pulses with excellent transverse coherence but limited temporal coherence. In fact, a typical SASE-FEL pulse consists of multiple uncorrelated spikes in both time and spectral domains. The relative bandwidth of the SASE-FEL pulses is on the order of the Pierce parameter [12], which for x rays is at the 10^{-3} level.

There are mainly two ways to improve the temporal coherence of SASE x-ray FELs: with seeding schemes and with slippage-enhancement methods. Fully coherent pulses can also be obtained by reducing the pulse duration to match one single spike [13–17], but in this case the temporal coherence and bandwidth are not improved. Seeding schemes typically amplify a coherent signal with narrow bandwidth, resulting in an improvement of the temporal coherence and a bandwidth reduction with respect to SASE. There are two main options for seeding: self-seeding and external seeding. In the self-seeding mechanism, a SASE pulse generated in a first undulator section passes through a monochromator before being amplified as a more coherent signal in a second undulator section. Self-seeding has been shown to work for soft and hard x rays [18,19]. Better results have been obtained for hard x rays: the bandwidth has been reduced by 2 orders of magnitude and pulses close to the Fourier limit have been generated [20]. External seeding employs optical lasers in combination with modulators and magnetic chicanes to produce coherent FEL radiation. External seeding is currently limited to the soft x-ray regime [21], and reaching hard x rays seems difficult due to wavelength limitations of available external lasers and noise degradation issues [22].

The temporal coherence of SASE-FELs can also be improved by enhancing the slippage of the radiation field. This can be achieved with harmonic lasing schemes, which so far have delivered moderate improvements in bandwidth (less than a factor of 2) in the soft x-ray regime [23,24]. Another option to increase the slippage length is by

*Contact author: eduard.prat@psi.ch

Published by the American Physical Society under the terms of the Creative Commons Attribution 4.0 International license. Further distribution of this work must maintain attribution to the author(s) and the published article's title, journal citation, and DOI.

delaying the electrons with respect to the photons with magnetic chicanes within the undulator. This was proposed in [25,26], putting forward two related schemes with different aims: mode-coupled SASE (MC-SASE) [25] and high-brightness SASE (HB-SASE) [26].

MC-SASE generates a set of longitudinal radiation modes by implementing a series of equal delay and slippage per undulator module. Each mode acquires spectral bands that overlap neighboring modes. The modes are coupled due to their collective interaction with the electron beam over regions of a coherence length, within which a series of regularly spaced radiation spikes of approximately uniform length may develop. The pulse duration of the modes is shorter than the SASE spikes since, due to the periodicity of the pulse pattern, the effective slippage occurs only within one undulator module (rather than in the entire undulator length as in SASE). Consequently, the spectral envelope of MC-SASE spanning all bands is larger than the SASE spectrum. The photon energy separation between the bands in the spectrum corresponds to the chicane delay (plus the slippage within one module), thus the spectral separation between the bands can easily be tuned by changing the magnetic strength of the chicanes.

The modes can be phase *locked* by introducing a modulation in the electron beam with the same period as the mode spacing, in the so-called mode-locked SASE [25]. The modulation can be achieved with an external laser with a wavelength matching the delay and slippage. The modulation favors the formation of spikes only in certain periodic regions of the bunch, resulting in a single temporal train of equally spaced pulses, in contrast to MC-SASE, where the spikes can develop at any position.

HB-SASE also uses several magnetic chicanes, but they are tuned to different delays. With the right setting of unequal delays, the spectral bands supported by each undulator and chicane can become unique in a way that only the frequencies at the resonant frequency will receive amplification. Simulations with isochronous chicanes (introducing only delay) show that the bandwidth can be improved by about 2 orders of magnitude with respect to SASE-FEL radiation, obtaining pulses close to the Fourier limit, while for standard dispersive chicanes (introducing delay and longitudinal dispersion) the improvements are limited to a factor of 10 [26]. In comparison to the seeding schemes, HB-SASE is more compact and cost-efficient, can potentially work at any wavelength or repetition rate, and does not require an external laser or a monochromator.

In both MC-SASE and HB-SASE, the undulator length of each module should be shorter than the FEL gain length for an efficient implementation of the schemes [25,26]. Although MC-SASE and HB-SASE were proposed more than a decade ago, to our knowledge an experimental demonstration has not been given yet. In this Letter we present a proof-of-principle experiment of the MC-SASE and HB-SASE schemes in an x-ray FEL, showing the production of frequency combs and narrow bandwidth FEL pulses.

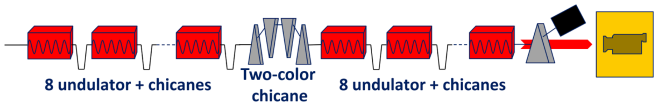


FIG. 1. Schematic layout of the SwissFEL Athos beamline (not to scale), adapted from Fig. 1 in [29].

The demonstration was performed in Athos [27], the soft x-ray beamline of SwissFEL [10]. A sketch of the Athos undulator beamline is shown in Fig. 1. The Athos undulator consists of 16 APPLE-X modules [28] capable of providing variable polarization and transverse gradient. Each module has a total length of 2 m, a period λ_u of 38 mm, and a maximum K value of around 3.8. There is a small magnetic chicane of 0.2 m between every two adjacent undulator modules. These intraundulator chicanes are the key components for MC-SASE and HB-SASE. The chicanes can also be employed to reduce the FEL saturation length via the optical klystron effect [29], or to generate high-power and short FEL pulses with the fresh-slice multi-stage amplification scheme [30]. In the middle of the undulator beamline there is a larger chicane for the production of widely tunable two-color FEL pulses [31].

The intraundulator magnetic chicanes consist of four dipoles and introduce both a delay and longitudinal dispersion, where the latter amounts to approximately twice the equivalent delay. The chicanes can give a maximum delay of about 5 fs (for an electron beam energy of 3.4 GeV), corresponding to 1.5 μm photon path length. From now on, we will refer to delays either in units of time or corresponding path length. The chicanes have sufficient precision to control the delay on a subwavelength scale and can therefore act as phase matchers. In case of using dispersive chicanes, like we have in Athos, the bandwidth improvement is limited to a factor of 10 [26], as already mentioned. The longitudinal dispersion also reduces the saturation length via the optical klystron effect [29], thus enabling a more compact FEL structure. In short, the dispersion accelerates the conversion from energy modulation to density modulation, or microbunching, in the FEL process. Simulations for Athos show that in the HB-SASE scheme the bandwidth can be improved by a factor of between 3 to 9 (for photon energies between 250 eV and 1.8 keV, respectively) and that the saturation length can be reduced by at least 20% [32,33].

We employed a photon spectrometer to measure the FEL spectra [34]. The dispersive element of the spectrometer is a grating monochromator with the dispersed spectrum at the exit slit imaged on a yttrium-aluminum-garnet screen viewed with a 2D CMOS detector. The photon energy is calibrated by photon absorption lines and the geometry of the spectrometer. We occasionally cross check the calibration by changing the photon energy with the undulator

field. The resolution of the spectrometer is expected to be better than 0.2 eV at a central photon energy of 500 eV. An x-ray gas monitor measures the FEL pulse energy [35].

The performance of MC-SASE and HB-SASE is very sensitive to the intrinsic energy spread and the energy chirp of the electron beam. The energy chirp refers to the slope in the variation of the mean energy along the longitudinal position (or time) of the electron beam, while the intrinsic energy spread refers to the variation of electron energy over a short longitudinal section of the bunch, averaged over the length of the bunch (uncorrelated energy spread). Smaller uncorrelated energy spread values are desired to enable larger delays without producing overbunching due to the longitudinal dispersion of the chicanes. Moreover, an energy chirp of the electron beam results in an energy chirp of the photon beam (the chirp of the photon beam is about twice the chirp of the electron bunch), which leads to an increase of the FEL bandwidth.

In standard operation the electron beam in Athos is compressed in three stages to a few kA. In the proof-of-principle demonstration shown here, in order to reduce both the uncorrelated energy spread and the energy chirp, we compressed the electron beam only in the first compression stage (a magnetic chicane) to a peak current of about 500 A. Since the uncorrelated energy spread of the electron beam increases at least linearly with the compression factor, by reducing the final peak current we can also reduce the final energy spread. While in standard operation the energy spread is about 1 MeV or higher [36], here we measured, using the optical klystron effect [36], energy spread values between 200 and 300 keV. Moreover, operating with a single compression stage gives us greater flexibility to minimize the energy chirp of the electron beam by changing the phase of the linear accelerators downstream of the bunch compressor.

For our demonstration we worked with the standard bunch charge of 200 pC and a final electron beam energy of 3.4 GeV. The undulator was set to photon energies between 500 and 600 eV in helical configuration. This photon energy range was chosen because SASE can saturate with the given parameters and available undulator length (saturation could not be reached at significantly higher photon energies), thus allowing a direct comparison between SASE and MC- and HB-SASE, and because the spectrometer resolution is optimal in this range. For MC-SASE, the delays of the intraundulator chicanes between the active undulator modules were set to the same delay. For HB-SASE, we implemented varying delays, which decrease monotonically along the undulator. Starting with larger delays allows us to take advantage of the optical klystron mechanism, and finishing with smaller delays avoids overbunching close to the saturation point. We employed eight chicanes, starting with the first chicane set to a maximum delay of around 2.5 to 3 fs and the last set to around 0.5 fs. We empirically tried many different delay configurations and optimized the phase matchers, aiming for the best configuration in terms of spectral bandwidth.

Figures 2 and 3 show the spectral results for standard SASE, MC-SASE, and HB-SASE for a central photon energy of around 578 eV. The measurements were done during the same experimental shift and under equivalent input beam conditions. We took 500 consecutive spectra for each case. The FEL process was close to the saturation point, with a pulse energy of around 70 μJ for all cases.

For MC-SASE, we used all the chicanes set to the same delay of 600 nm or 2 fs. As is evident from the figures, bands appear in this case, leading to a broader overall

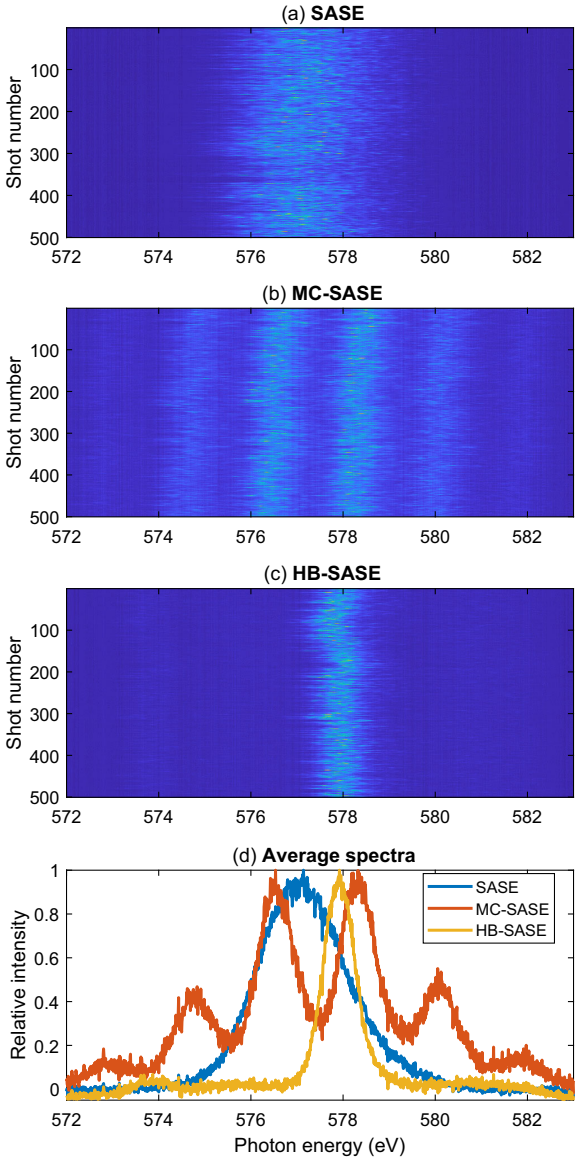


FIG. 2. Waterfall plot of 500 consecutive single-shot spectra for SASE (a), MC-SASE (b), and HB-SASE (c), and average spectra for the three cases (d). The horizontal axis is the same for all plots. Spectral intensities are shown relative to the maximum value in this figure and throughout the Letter.

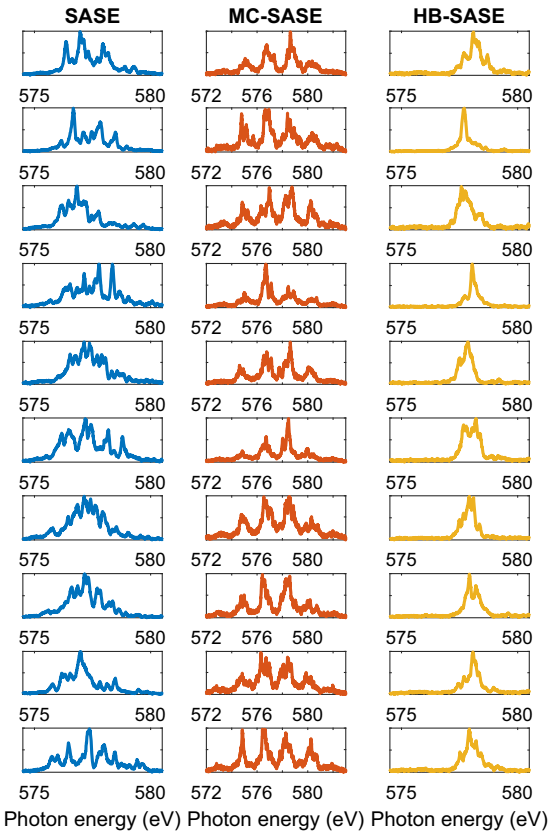


FIG. 3. Selected ten consecutive single-shot spectra from the dataset shown in Fig. 2 for SASE (left), MC-SASE (center), and HB-SASE (right). For better visibility the spectra for SASE and HB-SASE are displayed in a narrower photon energy window than MC-SASE.

spectrum compared to SASE. In MC-SASE, the spectral extent of the bands is determined more by the number of undulator periods per module (52 in our case, giving a total bandwidth of about $1/52$ or 1.9%, fitting well with the measured spectra). The broadening of the spectrum with respect to SASE reflects a shorter pulse duration of the MC-SASE modes in comparison to the SASE spike duration. The separation between the bands is about 1.76 eV and fits well with the expected value of the total delay within one module (710 nm or 1.75 eV): 600 nm delay of the chicane plus the slippage of around 110 nm (equal to the number of periods, 52, times the radiation wavelength, 2.15 nm).

For the HB-SASE case, we employed eight chicanes with the following delays in femtoseconds: 2.53, 1.85, 1.62, 1.31, 1.03, 0.83, 0.74, and 0.44. Varying the delays eliminates all but one band, resulting in a significant reduction of the bandwidth with respect to the SASE case. The single-shot bandwidths (rms values obtained from Gaussian fits) averaged over all shots (500) are 0.913 ± 0.161 eV for SASE, and 0.306 ± 0.062 eV for HB-SASE. With HB-SASE the bandwidth is reduced by a factor of 3.

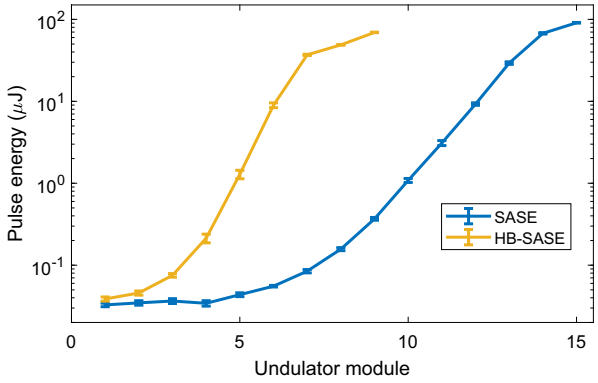


FIG. 4. Gain curves measured for the SASE and HB-SASE configurations corresponding to the spectra shown in Fig. 2.

Simulations for similar beam and undulator parameters as in the experiment show equivalent performance of HB-SASE (i.e., a bandwidth reduction of about a factor of 3).

The gain curves for the SASE and HB-SASE cases are shown in Fig. 4. We employed 14 undulator modules for SASE and nine for MC-SASE and HB-SASE to reach a pulse energy of about 70 μJ. Thus, considering that the FEL process is close to saturation for these pulse energies, the FEL saturation length is reduced by 36% thanks to the optical klystron mechanism. Such a reduction in saturation length is better than the results reported in [29,37], although here the focus is on improving the bandwidth and not only the saturation length as in [29,37]. The reason is that in this case the intrinsic energy spread is lower and the efficiency of the optical klystron improves for lower energy spread values. This result underlines the importance of having an electron beam with low energy spread to make better use of the optical klystron effect.

After demonstrating MC-SASE and HB-SASE, we will now focus on the tunability of MC-SASE. Figure 5 displays MC-SASE spectra as a function of different chicane delays (between 400 and 1400 nm), collected during a different experimental shift for a central photon energy of 500 eV. We used eight undulator modules for 400 nm delay and seven modules for all other delays. The pulse energy was between 50 μJ (1400 nm delay) and 80 μJ (400 nm delay). As expected the spectral envelope is similar for all cases but the separation between the bands, and thus the number of bands, depends on the implemented chicane delay: the separation between the bands varies between 2.23 eV (400 nm delay) and 0.74 eV (1400 nm delay), corresponding to between three bands (400 nm delay) to about ten bands (1400 nm delay). The difference between the measured band separations and the expected values (based on chicane delay plus slippage) is less than 10%.

To conclude, in the SwissFEL Athos beamline we have demonstrated two schemes that improve the temporal coherence of SASE-FEL pulses in the soft x-ray regime

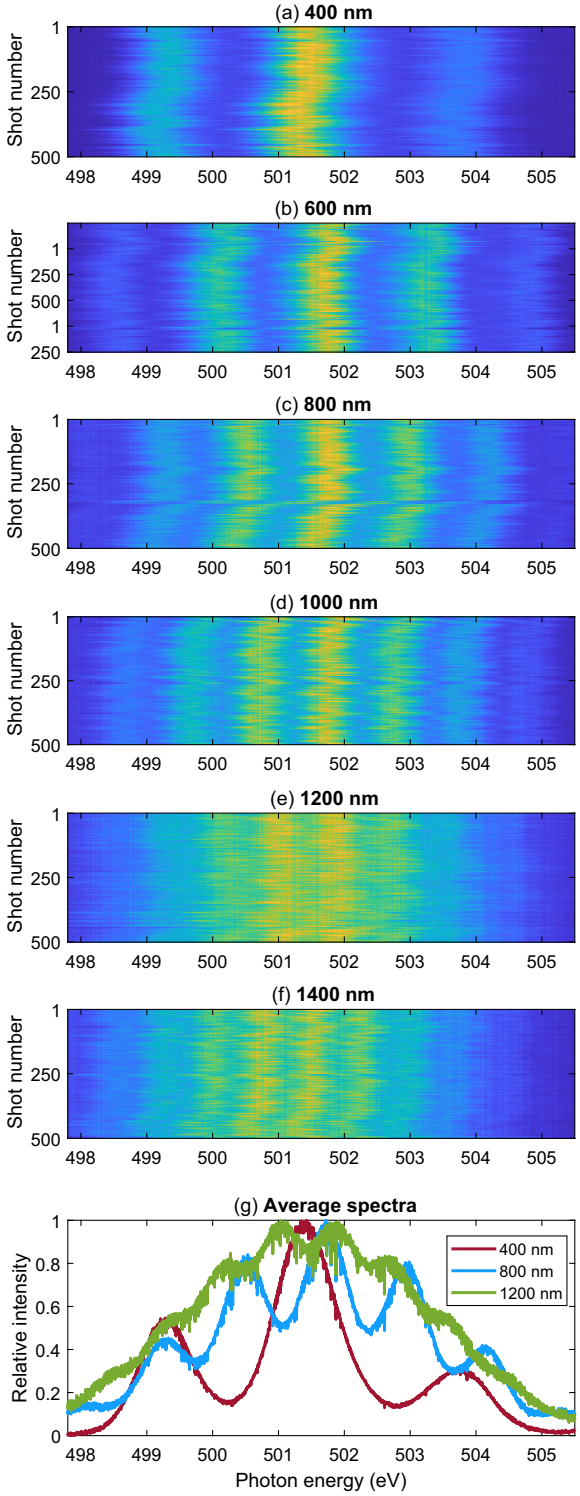


FIG. 5. Waterfall plot of 500 consecutive single-shot spectra of MC-SASE for different delays [(a) to (f)] and average spectra for some selected delays (g). The horizontal axis is the same for all plots.

by means of gradually delaying the electron bunch with respect to the radiation field and thus enhancing the slippage. With MC-SASE we generated frequency combs with tunability in the number and separation of the spectral peaks; with HB-SASE we produced FEL radiation with bandwidths reduced by up to a factor of 3 with respect to standard SASE pulses, while also reducing the saturation length by up to about 40%.

MC-SASE is also the basis for mode-locked SASE, for which we have already observed some evidence (see, e.g., [27]), but full proof is still missing. Future efforts at SwissFEL will be directed toward demonstrating mode-locked SASE, which may require time-resolved photon diagnostics, and improving the HB-SASE performance for higher peak currents and different photon energies. To achieve the latter, we may attempt a further reduction of the energy spread of the beam, improve the resolution of our spectrometers or use optimizers to find ideal undulator and chicane settings for best performance. For future facilities it may be beneficial to design the undulator beamline with shorter modules than in SwissFEL Athos and with compact isochronous magnetic chicanes in between. This would allow a further reduction of the bandwidth of MC-SASE and HB-SASE, with the potential to achieve true transform-limited pulses.

Our reported progress will be beneficial for current applications requiring frequency combs or reduced bandwidth such as resonant inelastic x-ray scattering [38], or any experiment utilizing a monochromator. X-ray frequency combs may have an impact on spectroscopy techniques, similar to the role frequency combs have played in the optical regime [39,40]. The work at Athos paves the way for further developments, such as the generation of mode-locked SASE and transform-limited pulses, which could bring further notable benefits to FEL science applications.

Acknowledgments—We thank Thomas Schietinger for improving the language and consistency of the manuscript. We acknowledge the support of all the technical groups involved in the operation of SwissFEL. W. H. is supported by funding from the European Research Council under the European Union's Horizon 2020 research and innovation program, within the Hidden, Entangled and Resonating Order (HERO) project with Grant Agreement 810451.

[1] B. W. J. McNeil and N. R. Thompson, Nat. Photonics **4**, 814 (2010).
[2] C. Pellegrini, A. Marinelli, and S. Reiche, Rev. Mod. Phys. **88**, 015006 (2016).
[3] C. Bostedt, S. Boutet, D. M. Fritz, Z. Huang, H. J. Lee, H. T. Lemke, A. Robert, W. F. Schlotter, J. J. Turner, and G. J. Williams, Rev. Mod. Phys. **88**, 015007 (2016).
[4] W. Ackermann, G. Asova, V. Ayvazyan, A. Azima, N. Baboi, J. Bähr, V. Balandin, B. Beutner, A. Brandt, A. Bolzmann *et al.*, Nat. Photonics **1**, 336 (2007).

[5] P. Emma, R. Akre, J. Arthur, R. Bionta, C. Bostedt, J. Bozek, A. Brachmann, P. Bucksbaum, R. Coffee, F.-J. Decker *et al.*, Nat. Photonics **4**, 641 (2010).
[6] T. Ishikawa, H. Aoyagi, T. Asaka, Y. Asano, N. Azumi, T. Bizen, H. Ego, K. Fukami, T. Fukui, Y. Furukawa *et al.*, Nat. Photonics **6**, 540 (2012).
[7] E. Allaria, D. Castronovo, P. Cinquegrana, P. Craievich, M. D. Forno, M. B. Danailov, G. D'Auria, A. Demidovich, G. D. Ninno, S. D. Mitri *et al.*, Nat. Photonics **7**, 913 (2013).
[8] H.-S. Kang, C.-K. Min, H. Heo, C. Kim, H. Yang, G. Kim, I. Nam, S. Y. Baek, H.-J. Choi, G. Mun *et al.*, Nat. Photonics **11**, 708 (2017).
[9] W. Decking, S. Abeghyan, P. Abramian, A. Abramsky, A. Aguirre, C. Albrecht, P. Alou, M. Altarelli, P. Altmann, K. Amyan *et al.*, Nat. Photonics **14**, 391 (2020).
[10] E. Prat, R. Abela, M. Aiba, A. Alarcon, J. Alex, Y. Arbelo, C. Arrell, V. Arsov, C. Bacellar, C. Beard *et al.*, Nat. Photonics **14**, 748 (2020).
[11] A. M. Kondratenko and E. L. Saldin, Part. Accel. **10**, 207 (1980), https://cds.cern.ch/record/1107977.
[12] R. Bonifacio, C. Pellegrini, and L. M. Narducci, Opt. Commun. **50**, 373 (1984).
[13] S. Huang, Y. Ding, Y. Feng, E. Hemsing, Z. Huang, J. Krzywinski, A. A. Lutman, A. Marinelli, T. J. Maxwell, and D. Zhu, Phys. Rev. Lett. **119**, 154801 (2017).
[14] A. Marinelli, J. P. MacArthur, P. Emma, M. W. Guetg, C. Field, D. Kharakh, A. A. Lutman, Y. Ding, and Z. Huang, Appl. Phys. Lett. **111**, 151101 (2017).
[15] A. Malyzhenkov, Y. P. Arbelo, P. Craievich, P. Dijkstal, E. Ferrari, S. Reiche, T. Schietinger, P. Juranić, and E. Prat, Phys. Rev. Res. **2**, 042018(R) (2020).
[16] J. P. Duris, J. P. MacArthur, J. M. Glownia, S. Li, S. Vetter, A. Miahnahri, R. Coffee, P. Hering, A. Fry, M. E. Welch *et al.*, Phys. Rev. Lett. **126**, 104802 (2021).
[17] E. Prat, A. Malyzhenkov, C. Arrell, P. Craievich, S. Reiche, T. Schietinger, and G. Wang, APL Photonics **8**, 111302 (2023).
[18] J. Amann, W. Berg, V. Blank, F.-J. Decker, Y. Ding, P. Emma, Y. Feng, J. Frisch, D. Fritz, J. Hastings *et al.*, Nat. Photonics **6**, 693 (2012).
[19] D. Ratner, R. Abela, J. Amann, C. Behrens, D. Bohler, G. Bouchard, C. Bostedt, M. Boyes, K. Chow, D. Cocco *et al.*, Phys. Rev. Lett. **114**, 054801 (2015).
[20] I. Nam, C.-K. Min, B. Oh, G. Kim, D. Na, Y. J. Suh, H. Yang, M. H. Cho, C. Kim, M.-J. Kim *et al.*, Nat. Photonics **15**, 435 (2021).
[21] P. R. Ribič, A. Abrami, L. Badano, M. Bossi, H.-H. Braun, N. Bruchon, F. Capotondi, D. Castronovo, M. Cautero, P. Cinquegrana *et al.*, Nat. Photonics **13**, 555 (2019).
[22] E. Saldin, E. Schneidmiller, and M. Yurkov, Opt. Commun. **202**, 169 (2002).
[23] E. A. Schneidmiller, B. Faatz, M. Kuhlmann, J. Rönsch-Schulenburg, S. Schreiber, M. Tischer, and M. V. Yurkov, Phys. Rev. Accel. Beams **20**, 020705 (2017).
[24] I. Nam, C.-K. Min, C. Kim, H. Yang, G. Kim, H. Heo, S. Kwon, S. H. Park, and H.-S. Kang, Appl. Phys. Lett. **112**, 213506 (2018).
[25] N. R. Thompson and B. W. J. McNeil, Phys. Rev. Lett. **100**, 203901 (2008).
[26] B. W. J. McNeil, N. R. Thompson, and D. J. Dunning, Phys. Rev. Lett. **110**, 134802 (2013).
[27] E. Prat, A. A. Haddad, C. Arrell, S. Augustin, M. Boll, C. Bostedt, M. Calvi, A. L. Cavalieri, P. Craievich, A. Dax *et al.*, Nat. Commun. **14**, 5069 (2023).
[28] T. Schmidt and M. Calvi, Synchrotron Radiat. News **31**, 35 (2018).
[29] E. Prat, E. Ferrari, M. Calvi, R. Ganter, S. Reiche, and T. Schmidt, Appl. Phys. Lett. **119**, 151102 (2021).
[30] G. Wang, P. Dijkstal, S. Reiche, K. Schnorr, and E. Prat, Phys. Rev. Lett. **132**, 035002 (2024).
[31] E. Prat, P. Dijkstal, E. Ferrari, R. Ganter, P. Juranić, A. Malyzhenkov, S. Reiche, T. Schietinger, G. Wang, A. A. Haddad, S. Augustin, C. Bostedt, G. Knopp, J. Knurr, A. S. Morillo-Candas, Z. Sun, and K. Schnorr, Phys. Rev. Res. **4**, L022025 (2022).
[32] E. Prat, M. Calvi, R. Ganter, S. Reiche, T. Schietinger, and T. Schmidt, J. Synchrotron Radiat. **23**, 861 (2016).
[33] E. Prat and S. Reiche, J. Synchrotron Radiat. **26**, 1085 (2019).
[34] C. Arrell, V. Thominet, Y. Arbelo, U. Wagner, N. Gradwohl, E. Prat, L. Patthey, and R. Follath, in *Conference on Lasers and Electro-Optics* (Optica Publishing Group, Washington, 2022).
[35] A. A. Sorokin, Y. Bican, S. Bonfigt, M. Brachmanski, M. Braune, U. F. Jastrow, A. Gottwald, H. Kaser, M. Richter, and K. Tiedtke, J. Synchrotron Radiat. **26**, 1092 (2019).
[36] E. Prat, C. Kittel, M. Calvi, P. Craievich, P. Dijkstal, S. Reiche, T. Schietinger, and G. Wang, Phys. Rev. Accel. Beams **27**, 030701 (2024).
[37] C. Kittel, M. Calvi, S. Reiche, N. Sammut, G. Wang, and E. Prat, J. Synchrotron Radiat. **31**, 948 (2024).
[38] A. Kotani and S. Shin, Rev. Mod. Phys. **73**, 203 (2001).
[39] T. Udem, R. Holzwarth, and T. W. Hänsch, Nature (London) **416**, 233 (2002).
[40] S. T. Cundiff and J. Ye, Rev. Mod. Phys. **75**, 325 (2003).